IEEE Access
Multidisciplinary ⋮ Rapid Review ⋮ Open Access Journal

Received 1 February 2024, accepted 9 February 2024, date of publication 13 February 2024, date of current version 23 February 2024.

Digital Object Identifier 10.1109/ACCESS.2024.3365938

RESEARCH ARTICLE

Design and Performance Measurement of Worn-on-Body Instrumental Ultra-Miniaturized UWB Wearable Patch for e-Health Monitoring

SUMON MODAK[1], (Member, IEEE), VIKRANT KAIM[2], (Member, IEEE), TAIMOOR KHAN[3], (Senior Member, IEEE), BINOD KUMAR KANAUJIA[4], (Senior Member, IEEE), LADISLAU MATEKOVITS[5,6,7], (Senior Member, IEEE), AND KARUMUDI RAMBABU[8], (Member, IEEE)

[1]Department of Electronics and Communication Engineering, National Institute of Technology Warangal, Warangal, Telangana 506004, India
[2]Department of Electronics and Communication Engineering, Faculty of Technology, University of Delhi, Delhi 110007, India
[3]Department of Electronics and Communication Engineering, National Institute of Technology Silchar, Silchar, Assam 788010, India
[4]Department of Electronics and Communication Engineering, Dr. B. R. Ambedkar National Institute of Technology Jalandhar, Jalandhar, Punjab 144011, India
[5]Department of Electronics and Telecommunications, Politecnico di Torino, 10129 Turin, Italy
[6]Istituto di Elettronica e di Ingegneria dell'Informazione e delle Telecomunicazioni, National Research Council of Italy, 10129 Turin, Italy
[7]Measurements and Optical Electronics, Politehnica University Timişoara, 300006 Timişoara, Romania
[8]Department of Electrical and Computer Engineering, University of Alberta, Edmonton, AB T6G 2R3, Canada

Corresponding author: Ladislau Matekovits (ladislau.matekovits@polito.it)

This work was supported by the Science and Engineering Research Board (SERB), Government of India, through the Visiting Advanced Joint Research (VAJRA), Government of India, in July 2020, under Grant VJR/2019/000009.

ABSTRACT A conformal, ultra-miniaturized, circuit integrated ultra-wideband (UWB) coplanar-waveguide (CPW) antenna system for worn-on-body applications is developed in this article. The performance study of the proposed antenna is performed over a four-layer human body tissue model. A shortened ground plane and a pair of L-shaped stubs are included to the umbrella-shaped patch configuration to enhance the impedance bandwidth between 3.15-10.55 GHz, which encompass a variety of applications like WiMAX band (3.3-3.8 GHz), WLAN band (5.150-5.350 GHz), unlicensed ISM band (5.725-5.875 GHz), and X-band (7.250-7.745, and 7.900-8.395 GHz). The realization of wideband behavior for the reported antenna is studied using the characteristic mode theory (CMT). A maximum peak gain of 4.2 dBi is achieved with maximum radiations in broadside with higher front-to-back ratio in both E-plane and H-plane. Furthermore, the robustness of the proposed antenna is evaluated by studying its performances under different conditions, such as using a coaxial feeding system, bending and assessing SAR levels. The antenna is fabricated and assembled with various circuit components to validate its performance with the simulated counterpart. The experiment is carried out by placing the antenna structure over different parts of the human body. Finally, a comparative analysis is carried out and it is found that the proposed antenna exhibits 98.2% compactness than the existing antenna designs available in the literature.

INDEX TERMS Characteristic mode theory, coplanar-waveguide antenna, conformal, ultra-miniaturized ultra-wideband, umbrella design, wearable.

I. INTRODUCTION

Over the past decades, the development of UWB technology has evolved to a great interest among researchers due to its advantages, such as low spectral density, low power consumption, low cost, and high data rates [1]. Since the release of unlicensed band 3.1-10.6 GHz by FCC in 2002, the research in UWB has seen manifold advantages targeting different operational modules and connectivity strategies [2]. As a fundamental part of the UWB communication system, antennas have drawn considerable attention and have aroused much popularity. Nevertheless, most of the antennas

The associate editor coordinating the review of this manuscript and approving it for publication was Pavlos I. Lazaridis.

are unsuitable for UWB communications due to design complexity, and substantial size. Antenna designs reported in [3], [4], [5], and [6] are based on circular and elliptical-shaped patches integrated with various resonant structures to accomplish wide frequency bands of operation. A novel CPW feed patch antenna configuration featuring a circular and elliptical-shaped stub is presented in [7]. The antenna operates within the frequency band of 3.1-10.6 GHz. Yan et al. [8] proposed a circularly polarized wideband umbrella-shaped patch antenna by modifying an elliptical-shaped radiator. Likewise, utilizing different slotted geometry over the patch and ground layer of umbrella-shaped antenna designs in [9] and [10], a wide operational bandwidth of 3.1-13.4 GHz, and 7.5-12.5 GHz is retained, respectively. Although the reported designs in [7], [8], [9], and [10] have achieved an acceptable impedance bandwidth but suffer from several constraints like non-medical applications, design complexity, large circuital area, and non-flexible geometry. Indeed, UWB technology also seems to be a good candidate for on-body networks and has much popularity in wireless biotechnologies [11]. Therefore, in the context of WBAN applications, antennas have drawn significant attention over the past few years. The idea behind the development of wearable antennas has acquired several applications in health care monitoring, smart home, telemedicine, sports, military, etc. In recent years, research on wrist-worn wireless communication devices has been tremendously increased for applications in smartwatches and smart wristbands, [12], [13]. Two different configurations of wearable antenna systems is proposed for smartwatch applications in health care monitoring [14], [15]. Chen et al. [16] have developed an inverted L-shaped antenna configuration with a high-impedance surface. A dual-port circular MIMO antenna designed for smartwatch applications is presented based on characteristic mode theory. The antenna is tailored to operate within the 2.4-2.49 GHz range, covering both Wi-Fi and Bluetooth bands [17]. A four-port MIMO antenna configuration is integrated into the watchstrap for smartwatch applications, operating in the frequency range of 5.2-5.8 GHz [18].

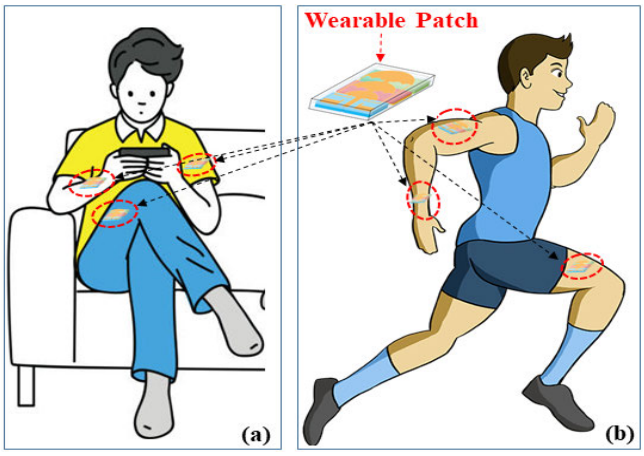

FIGURE 1. Wearable patch-based health monitoring system under different environmental conditions (a) Indoor, (b) Outdoor.

Noteworthy, as the wearable antennas are intended for body- worn applications, it is highly desirable to have flexible characteristics in order to suitably fit on human body parts that result in avoiding collision with other rigid substances which will protect the antenna structure from damage. A substantial amount of work has been done in developing flexible antenna structures for various wearable applications [19], [20]. UWB antenna with a flexible substrate operating within 4-6 GHz is designed for the detection of breast cancer [21] Similarly, for applications in the textile domain, a low-profile microstrip antenna modeled on denim jeans is introduced for wide-frequency UWB communications [22]. A four-port footwear wearable antenna structure is developed by Jayant et al. [23]. The suggested antenna possesses a flexible structure and operates between 2-14 GHz. Although in the reported antenna structures a significant performance has been obtained in terms of operational bandwidth, gain, and flexibility, but the antenna structures presented in [21] and [22], are larger in size, which makes them unsuitable for small movable parts of the body like wrist, fingers, and toes. In addition, the curvature effect and specific absorption rate (SAR) analysis has not been studied which is a major concern in case of wearable and flexible antenna structures. Likewise the antenna proposed in [23] exceeds the limit of compactness due to its implementation in footwear which has high risk of getting damaged. Therefore, to address the above constraints, a coplanar flexible ultra-miniaturized circuit integrated UWB antenna system intended to be operational over different parts of human body (wrist, biceps, and thigh) is presented for health care monitoring applications. The targeted operational scenario for the proposed wearable antenna in indoor and outdoor environments is illustrated in Fig. 1. This shows that the wearable patch (circuit integrated antenna) will collect relevant physiological data in different environments using biosensors and will process the data through analog signal conditioning and digital processor; finally the processed information will be transmitted wirelessly to the external base station [24]. The performance of the proposed antenna is evaluated through simulations over a four-layer human body tissue model. It offers distinct advantages over existing literature, including (i) remarkable compactness (98.2% compact in comparison to antenna structure in ref. [21]), (ii) utilization of characteristic mode theory to enhance impedance bandwidth, and (iii) a broad operational bandwidth ranging from 3.15 to 10.55 GHz. Furthermore, the robustness of the proposed antenna is thoroughly evaluated under diverse scenarios. This includes an examination of the antenna's performance in bending scenarios, an assessment of its performance behavior in proximity to the coaxial feeding system, and measurements of SAR. This comprehensive analysis provides insights into the antenna's durability and suitability for practical applications in different conditions. The novel features of the proposed antenna are compared with the existing literature and presented in Table 1. The paper is divided into the following six sections. The introduction is presented in Section I.

TABLE 1. Comparison of the proposed wearable patch with state-of-the-art.

Ref.	Substrate	Monopole Design	Antenna Size (mm^3)	System Analysis	Operating Freq. (GHz)	Freq. Band	CMT Study	Conformal	SAR (W/kg)	Peak Gain (dBi)	Applications
[14]	FR4 Epoxy	L-Shaped	44×15×1.6 (= 1056)	No	5.11-5.8	ISM	No	Yes	0.57	4.52	Smartwatch
[15]	FR4 Epoxy	Circular	30×30×1.6 (= 1440)	No	MNB	NA	No	No	2, 4	6.6	Smartwatch
[16]	FR4 Epoxy	Inverted L-Shaped	38×38×2 (= 2888)	No	2.38-2.5	ISM	No	No	0.29	6.3	Smartwatch
[17]	FR4 Epoxy	CAR	NA	No	2.4-2.49	ISM	No	No	NA	3.5	Smartwatch
[18]	Polyamide	Rectangular Strip	40×38×8 (= 12160)	No	5.2-5.84	ISM	No	Yes	NA	3.3–5.6	Smartwatch
[21]	Phenylthiophene	Rectangular	20×14×1.6 (= 448)	No	4-6	ISM	No	No	NA	1	Wearable Bra
[22]	Denim Jeans	Edge truncated	36×29×2 (= 2088)	No	3-11	UWB	No	No	NA	7.2	BAN
[23]	Polyethylene	Dome Shaped	92×92×1.5 (= 12696)	No	2-14	UWB	No	Yes	0.001	7.2	Footwear
This Work	**Polyimide (Flexible)**	**Umbrella Shaped**	**16×10×0.05 (= 8)**	**Yes**	**3.15-10.55 2.71-10.56 3.29-10.53**	**UWB**	**Yes**	**Yes**	**1.99 1.96 2.04**	**4.2 (overall)**	**Wrist Biceps Thighs**

CAR: Circular Annular Ring. MNB: Multi Narrow Bands; NA: Not Available; BAN: Body Area Network, SAR: Specific Absorption Rate (W/kg), Peak Gain (dBi)

The geometrical design of the reported prototype structure and its evolution process is discussed and analyzed using CMT in Section II. Section III outlines the simulated performance and sensitivity analysis.

The measurement scenario and the experimental validation is covered in Section IV. The SAR analysis for the reported wearable patch is presented in Section V, and the conclusion is drawn in Section VI.

II. WEARABLE PATCH

A. INTEGRATED ANTENNA SYSTEM DESIGNS

Fig. 2(a) illustrates the proposed antenna geometry which exhibits an overall dimension of 16×10 × 0.05 mm^3. The other dimensions in mm are as follows: $L_s = 16$, $W_s = 10$, $R = 4.8$, $R_1 = 1$,$W_f = 1$, $L_f = 10$, $L_1 = 8$, $L_2 = 3.8$, $C = 1.6$, $C_1 = 0.1$, $L_g = 2$, $Wg = 3$. The designed antenna comprises a triple-stacked umbrella patches acting as a radiator and a shortened ground layer. Both patch and ground layers are coplanar on the conformal and biocompatible substrate polyimide having relative permittivity, $\varepsilon_r = 4.3$ and thickness = 0.05 mm. Fig. 2(b) shows the isometric view of the proposed antenna fed with coaxial feed system. Fig. 3(a) shows the exploded view of the proposed wearable patch (antenna integrated with different circuitry components). The electronic components are integrated over another polyimide layer; and placed at the backside of the antenna substrate. The dimensions of various components are: biosensor pack (4.5 × 4.5×0.1 mm^3) power supply unit (10×4 × 0.05 mm^3), data unit (10×4 × 0.05 mm^3), memory unit (5.5 × 4.5×0.1 mm^3), and battery (6.5 × 4.5×1.2 mm^3).

Noteworthy, the integrated antenna system is designed in such a way that the antenna layer is placed over the circuitry layer with zero gap in-between; and both the layers are packed together and enclosed with a polyimide (biocompatible) layer. During simulation, the battery is represented as a perfect electric conductor (PEC), whereas all other circuit components are represented as dielectric [25]. Moreover, as the proposed antenna is applicable for body-worn purpose, it is important to consider the effects of human tissues. To that regard, all the simulations are carried out by placing the integrated antenna structure over a four-layer human body

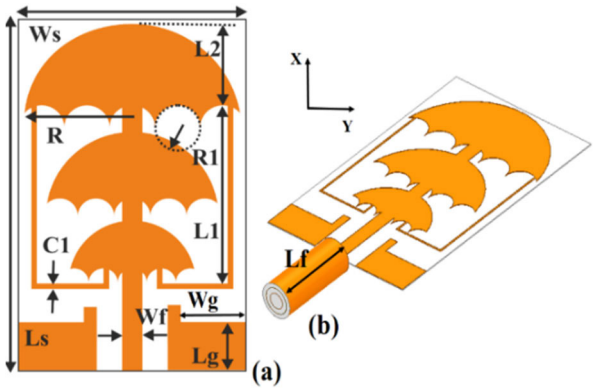

FIGURE 2. Proposed antenna geometry (a) Top view, (b) Isometric view with coaxial feed system.

tissue model which comprises skin ($\varepsilon_r = 37.45$, $\sigma = 1.74$), fat ($\varepsilon_r = 5.22$, $\sigma = 0.130$), muscle ($\varepsilon_r = 52.0$, $\sigma = 2.14$), and bone ($\varepsilon_r = 11.06$, $\sigma = 0.506$), in a cubic configuration having overall size 120 × 120× 50 mm^3.

The radiation boundaries (500 × 500×500 mm^3) are kept at a distance $\gg \lambda_0/2$ (at 3 GHz) from the antenna edges as depicted in Fig. 3(b). The electrical properties of different tissue layers are considered corresponding to the lowest frequency (3 GHz) of the ultra-wideband [26].

B. ANTENNA DESIGN EVOLUTION

The evolution process for the reported antenna is displayed in Fig. 4. The reflection coefficient ($|S_{11}|$) plot comparison for Ant-1, Ant-2, and Ant-3 are displayed in Fig. 5(a) whereas, comparison for Ant-4, Ant-5, and Ant-6 is shown in Fig. 5(b). Initially, an umbrella-shaped patch antenna (Ant-1) is designed by modifying a semi-circular shaped radiator with multiple circular slots at the edges. The ground layer is coplanar with the patch radiator. Ant-1 resonates at 4.3 GHz with -10 dB impedance bandwidth from 3.25-5.5 GHz, covering WiMAX, and WLAN bands. Since, designing an UWB antenna system to operate within a spectrum of 3.1-10.6 GHz is the target goal; therefore, to enhance the bandwidth two additional umbrella-shaped radiators of decreasing overall size are vertically stacked beneath the first radiator as shown in Figs. 4(b) and 4(c), which are termed as Ant-2

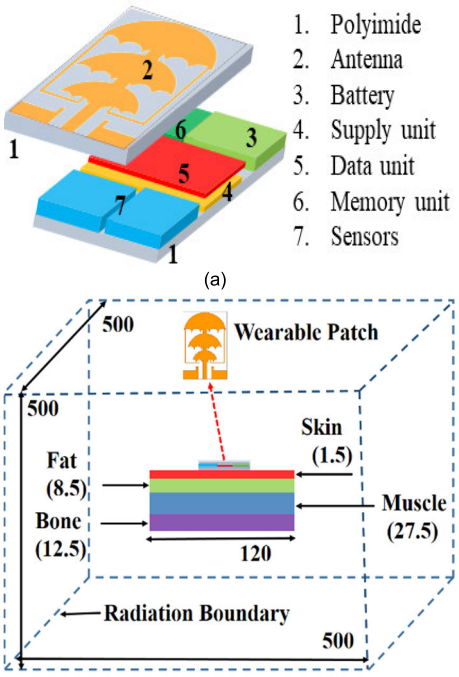

FIGURE 3. (a) Exploded view of the proposed antenna integrated with different circuitry components, (b) Human body tissue model.

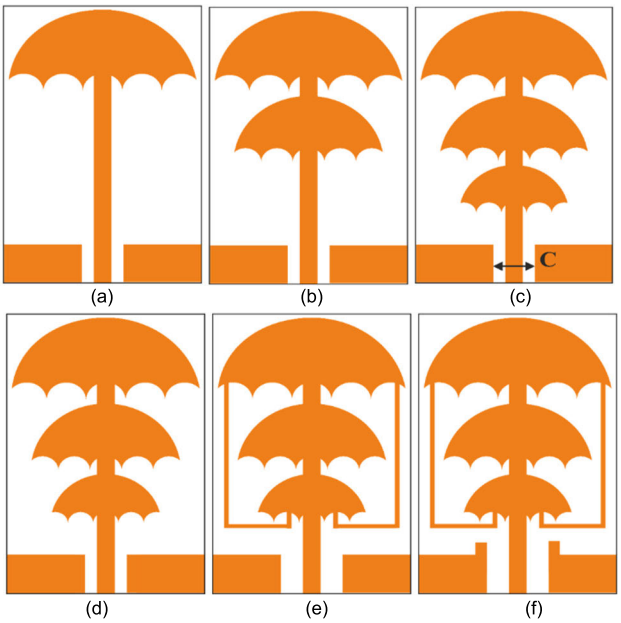

FIGURE 4. Antenna design evolution steps (a) Ant-1, (b) Ant-2, (c) Ant-3 (d) Ant-4, (e) Ant-5, and (f) Ant-6 (proposed).

and Ant-3, respectively. Consequently, the antenna operates within frequency band of 3.25-6.05 GHz, and 3.5-6.35 GHz respectively. Noted, compared to other antenna structure shapes such as, rectangular, circular, elliptical, etc., the umbrella-shaped structure offers higher impedance bandwidth due to larger (curved edges) antenna radiator's effective length [9]. Further, by increasing the separation between the ground plane in Ant-4; the modified ground improved the $|S_{11}|$ at lower frequency (~3 GHz) but the $|S_{11}|$ at higher frequency (~6 GHz) remains intact. Subsequently, to attain the target frequency spectrum, two L-shaped stubs are introduced connecting the umbrella-shaped patch at the top and bottom in Ant-5. The L-shaped stubs increase the patch's electrical length, which aids in enhancing the broad impedance bandwidth from 3.3-9.4 GHz in Ant-5. Finally, by truncating the ground plane in Ant-6 by length (Wg), the desired operating frequency spectrum of 7.4 GHz (3.15-10.55 GHz) is achieved. The design stages of Ant-1 to Ant-6 are summarized in Table 2. Noted, the design simulations for Ant-1 to Ant-6 are carried out in the presence of circuit elements.

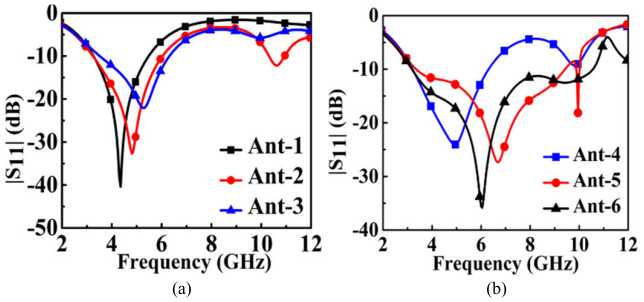

FIGURE 5. Comparison of simulated $|S_{11}|$ (a) Ant-1 to Ant-3, (b) Ant-4 to Ant-6.

TABLE 2. Antenna design stages.

Design Steps	Geometrical Description with	Operating Band (GHz)	Peak Gain (dBi)
Ant-1	Single Umbrella with IS	3.25-5.5	0.43 @5.4 GHz
Ant-2	Dual Umbrella with IS	3.25-6.05	0.75 @5.8 GHz
Ant-3	Triple Umbrella with IS	3.5-6.35	1.12 @6.1 GHz
Ant-4	Ground plane separation	3.2-6.35	1.29 @6.3 GHz
Ant-5	Addition of L-shaped stubs	3.3-9.4	3.36 @9.3 GHz
Ant-6	Truncated ground plane	3.15-10.55	4.2 @10.4 GHz

IS: Integrated System

C. EQUIVALENT CIRCUIT MODEL

In the context of ultra wideband (UWB) antenna design, matching bandwidth is attainable through the incorporation of multiple nearby resonances. Each of these resonances can be effectively modeled using parallel RLC tank circuit arranged in a series configuration [3], [27]. Hence, for a clearer comprehension of the resonance characteristics, an equivalent circuit model for the proposed antenna structure is established by interconnecting three parallel RLC resonance circuits based on three resonance modes in the frequency band of 3.15-10.55 GHz. Further, to address the impedance transformation resulting from feed inductance and static capacitance of the antenna, additional lumped components L_o and C_o are incorporated in the circuit. Moreover, to comprehensively analyze the equivalent circuit system, it is imperative to incorporate the coupling between the radiating modes. This intermode coupling is accurately modeled by introducing LC series lumped elements as defined in [28], [29], and [30]. The representation in Fig. 6(a) illustrates the equivalent resonance circuit model associated with the novel umbrella-shaped ultra wideband (UWB) antenna. The circuit model has been simulated employing a commercial

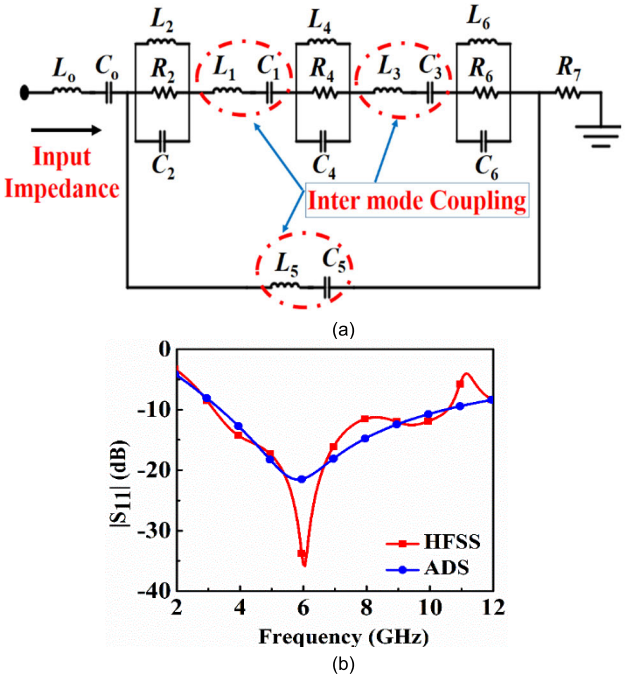

FIGURE 6. (a) Equivalent circuit model for the proposed antenna, (b) Comparative $|S_{11}|$ plot for the proposed umbrella shaped UWB antenna.

advanced design system (ADS) software. The values of all the components are as follows: $L_o = 0.21$ nH, $C_o = 3.18$ pF, $L_1 = 0.42$ nH, $C_1 = 9$ pF, $L_2 = 0.25$ nH, $C_2 = 0.24$ pF, $R_2 = 3.78\ \Omega$, $L_3 = 0.15$ nH, $C_3 = 1.31$ pF, $L_4 = 0.2$ nH, $C_4 = 0.23$ pF, $R_4 = 4.6\ \Omega$, $L_6 = 0.85$ nH, $C_6 = 0.23$ pF, $R_6 = 2.4\ \Omega$, $L_5 = 0.68$ nH, $C_5 = 0.22$ pF, $R_7 = 50\ \Omega$. Fig. 6(b) presents a comparative analysis of the $|S_{11}|$ parameters obtained from simulations conducted using HFSS and ADS. The results from both the simulators validates excellent agreement within the specified frequency band of 3.15-10.55 GHz.

D. PERFORMANCE ANALYSIS USING CHARACTERISTIC MODE THEORY

The effectiveness of the suggested antenna using characteristics mode theory (CMT) is discussed in this section. The theory of CMs was initially introduced to provide a more deterministic antenna design approach than the arbitrary or trial-error design approach. For a better understanding of mode characteristics, some equations are described below, which emphasize that the electric current ($\vec{J}$) on the surface of the conducting element is characterized by Eq. (1) as a sum of eigen current ($\vec{J}_n$) with weighted coefficients [31].

$$\vec{J} = \sum_n \alpha_n . \vec{J}_n \tag{1}$$

where, α_n is the modal weighting coefficient which can be obtained using Eq. (2):

$$\alpha_n = \frac{V_n^i}{1 + J\lambda_n} \tag{2}$$

where, V_n^i is the modal excitation coefficient and can be expressed by Eq. (3), where, $\vec{E}_i$ is the impressed source.

$$V_n^i = \left(\vec{J}_n . \vec{E}_i\right) \tag{3}$$

When a mode is excited at its resonating frequency, it radiates maximum power, i.e. $\lambda_n = 0$. Therefore, Eq. (2) can be rewritten as $\alpha_n = V_n^i$, meaning that when $\lambda_n = 0$, the modal weighting coefficient is equal to the modal excitation coefficient, and the modal significance (MS) is defined by Eq. (4):

$$MS_n = \left| \frac{1}{1 + J\lambda_n} \right| \tag{4}$$

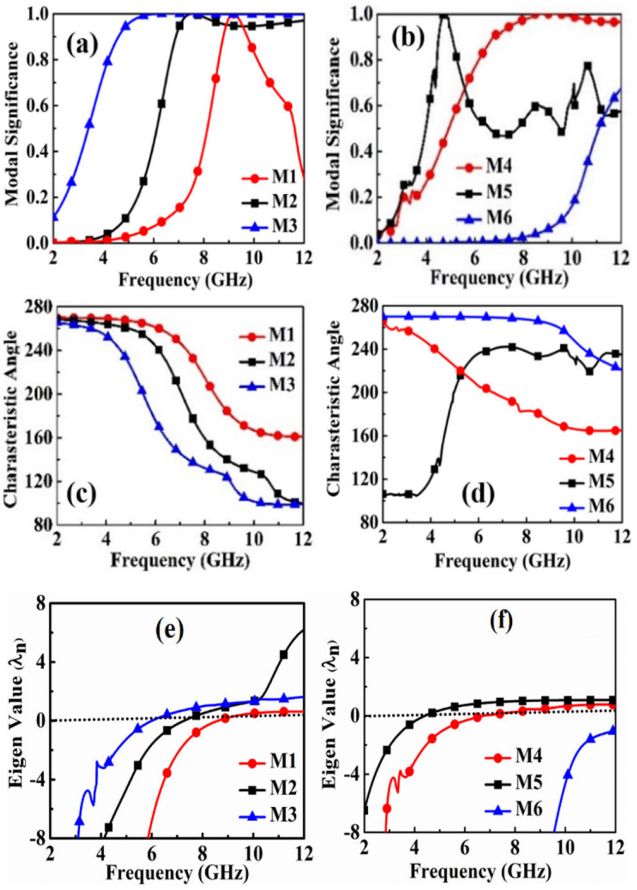

FIGURE 7. Modal Significance: (a) Modes M1-M3, (b) Modes M4-M6, Characteristics Angle: (c) Modes M1-M3, (d) Modes M4-M6, Eigenvalue (λ_n): (e) Modes M1-M3, and (f) Modes M4-M6.

Moreover, the approach of CMT provides a clear insights into antenna resonance, radiation mechanism, and serves as a pivotal tool to accumulate the existing modes inherent in the reported antenna geometry [32]. Besides, the adoption of CMT by various commercial electromagnetic solvers contributes to a more deterministic approach to antenna design, markedly distinct from the conventional arbitrary or trial error methods. In recent years, the use of characteristic modes for bandwidth enhancement has also been investigated [33], [34]. However, the literature on bandwidth enhancement using CM is minimal, and the physical phenomena have not been

discussed. Hence, in this section, the authors have tried to emphasize the existing mode present in the reported antenna by thorough discussion of the design approach using CMs. The CMs simulation for the reported antenna structure is carried out using CST microwave studio. Fig. 7 demonstrates that the suggested antenna is exciting six different modes, out of which five modes are considered to be significant modes that contribute strong radiation.

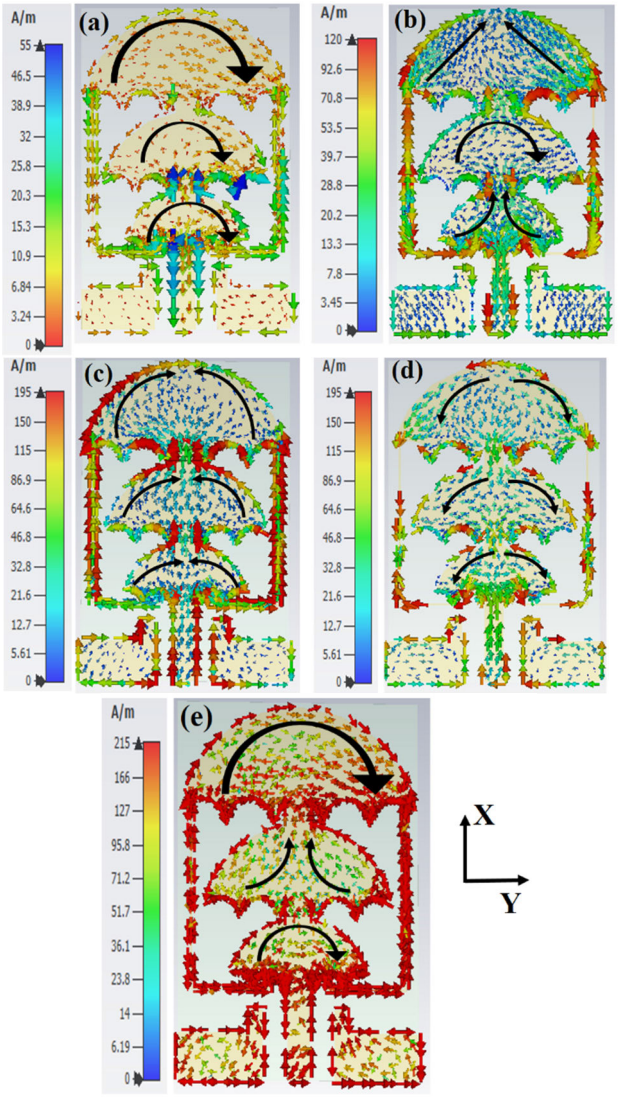

FIGURE 8. Simulated modal Current distributions at their respective mode: (a) J_1 at 9.2 GHz, (b) J_2 at 7.5 GHz, (c) J_3 at 5.9 GHz, (d) J_4 at 8.7 GHz, and (e) J_5 at 4.7 GHz.

Figs. 7(a) and 7(b) depicts the modal significance curves where mode M1 is resonating at 9.2 GHz showing a large modal significance value of 1. Similarly, the modes M2, M3, M4, and M5 also show large modal significance values around 1 at their respective resonant frequency 7.5, 5.9, 8.7, and 4.7 GHz, respectively. Meanwhile, mode M6 is a non-significant mode that provides weak radiation. Besides, utilizing the analysis of characteristic angle (α_n) and Eigen value (λ_n) the radiation properties of the antenna can be determine. This signifies that when $\alpha_n = 180°$, and $\lambda_n = 0$ the antenna actively radiates energy, otherwise the antenna stores electric and magnetic energy and behave as a capacitive and inductive. Hence, from Fig. 7(c), and Fig. 7(d) it can be observed that the modes M1-M5 intersect at 180° at their respective resonant frequencies within the UWB (3.1-10.6 GHz) frequency band. This lead to the conclusion that at the resonant frequency, modes M1-M5 demonstrates a tendency to effectively radiate EM energy. Meanwhile mode M6 has a higher value which is beyond the required frequency spectrum. Likewise, the electromagnetic (EM) radiation properties of an antenna can be visualized using the eigenvalues (λ_n). A resonance mode is indicated when $\lambda_n = 0$. It can be clearly visualize from Figs. 7(e) and 7(f) that modes M1 to M5 are resonating modes whose eigenvalues correspond to zero at their respective resonating frequencies. The modal currents for the dominant mode (M1-M5) are examined and represented as J_1, J_2, J_3, J_4, and J_5, for a clear analysis of the antenna's radiation mechanism (see Fig. 8). The dispersal of currents over the antenna structure leads to generating odd and even modes.

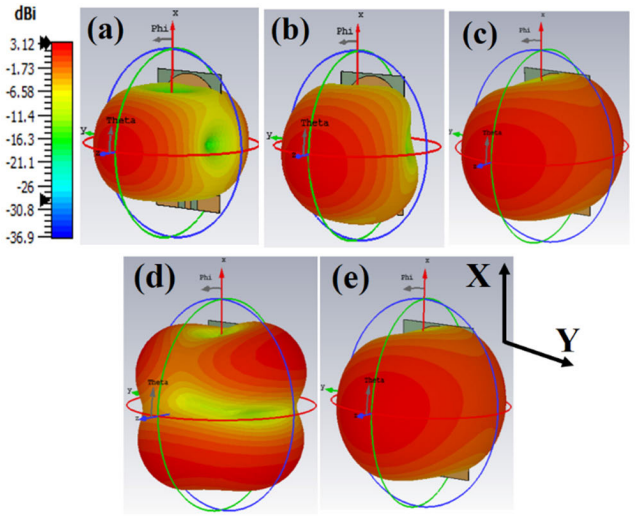

FIGURE 9. Directivity patterns for different frequency modes: (a) 9.2 GHz, (b) 7.5 GHz, (c) 5.9 GHz, (d) 8.7 GHz, and (e) 4.7 GHz.

The distributions of modal currents J_1 in all three umbrella-shaped radiators for mode M1 are in phase, which ensures mode M1 is an even mode [35]. Similarly, modes M3 and M4 are also the even modes that follow identical distributions of modal currents (J_3 and J_4) in the antenna radiator (See Figs. 8(c), and 8(d)). However, in modes M2 and M5 antiphase modal current (J_2 and J_5) patterns are noticed, rendering odd modes. Hence, the strategic excitation of consecutive odd and even modes within the suggested antenna design emerges as a key factor contributing to its wideband performance within the UWB spectrum of 3.15-10.55 GHz [36]. From Fig. 8, the modal currents J_1 to J_5 are mainly concentrated on the L -shaped stubs fol-

lowed by the feedline and gently flow through the antenna radiators. In the case of mode M1, the current is horizontally directed in all three umbrella-shaped radiators marked with a black arrow. In modes M3 and M4, the current direction is vertical, upward, and downward. An arbitrary flow of current in modes M2 and M5 is observed. Despite a strong current concentration at the ground layer in the form of a loop that tends to achieve broadside radiation behavior. The 3D radiation patterns for the reported antenna at five different modes are depicted in Fig. 9. It is obvious that Mode M1 and M2 provide maximum radiation in the z-direction appearing null at the central position in Y-axis. Whereas Mode M3 and M5 provide a good omnidirectional radiation pattern, and Mode M4 presents a radiation pattern with minimum radiations in X and Y-axis. Therefore, as a result, these five modes contribute more radiation in wideband operations.

III. SIMULATED PERFORMANCE

A. PARAMETRIC ANALYSIS

As the L-shaped stubs and ground plays an important role in obtaining the targeted frequency response of the proposed antenna, therefore, to observe the effect of the width of L-shaped stubs on the reflection coefficient of the proposed antenna, parametric variation of the stub width (C_1) has also been performed and mapped in Fig. 10(a).

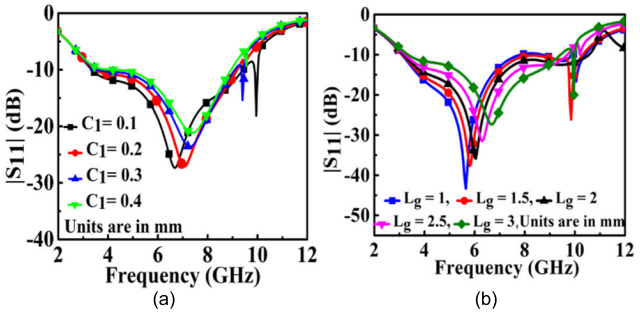

FIGURE 10. Comparison of simulated $|S_{11}|$ for parametric variation of (a) C_1 (width of L-shaped strip), and (b) Lg (length of ground plane).

It can be seen, even slight increment in the value of C_1 can detune and simultaneously shift the overall resonance towards higher frequency; and moreover, stub width has the potential to mismatch the impedance drastically, if width would not be optimized. Hence $C_1 = 0.1$ mm is considered to be the optimized width. Further, Fig. 10(b) shows the tuning effect on $|S_{11}|$ due to parametric variation of the ground plane's length (L_g). With an increment of 0.5 mm in the value of L_g from 1 to 3 mm, the overall resonance is shifting towards high frequency with the potential impedance mismatch. Thus, the optimized value of L_g is 2 mm, which makes the suggested antenna operate in a designated frequency band in order to be applicable for appropriate transfer of data related to the human body physiological statistics.

B. INTEGRATED ANTENNA SYSTEM ROBUSTNESS

In order to analyze sensitivity of the wearable patch, simulated performance of the proposed integrated antenna system is scrutinized by loading a coaxial feed of different cable length (L_f = 5 mm, 10 mm and 15 mm), as shown in Fig. 11 (a-c). Such analysis could support the actions to be taken in measurement procedure to validate this in-house prototype for the real-time application. The simulated $|S_{11}|$ comparison for different coaxial cable length (L_f) is mapped in Fig. 12(a).

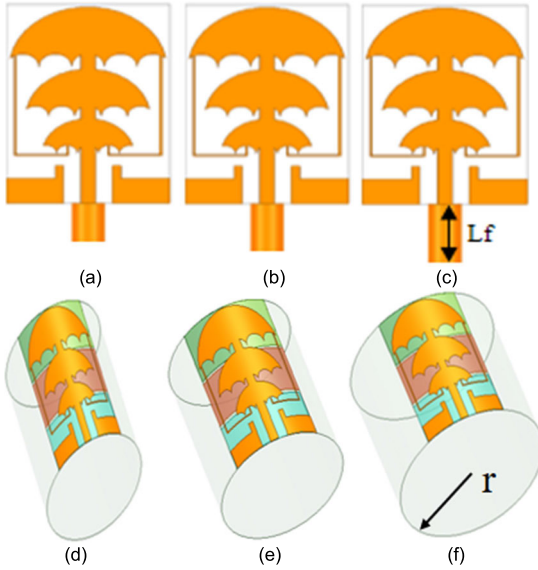

FIGURE 11. Coaxial feed length: (a) $L_f = 5$ mm, (b) $L_f = 10$ mm, (c) $L_f = 15$ mm, Antenna bending radii: (d) $r = 85$ mm, (e) $r = 150$ mm, (f) $r = 250$ mm.

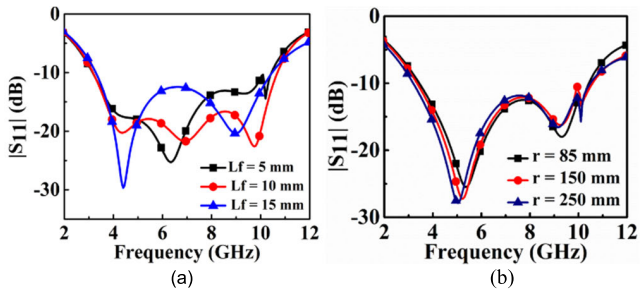

FIGURE 12. Comparison of simulated $|S_{11}|$ for parametric variation of (a) L_f (coaxial feed length) and, (b) r (antenna bending radii).

The comparative results suggest that the overall target impedance bandwidth remains intact due to the UWB profile of the antenna. Note input impedance is varying throughout the bandwidth for different cable lengths, as the intensity of the coupled current from the patch to the cable depends on the coaxial feed length. Further, robustness of the wearable patch is also analyzed due to the curvature effects which could arise in its real-time application. As the proposed antenna system is built on flexible polyimide substrate, it could easily adapt to the curved surface of its intended location (wrist, biceps and thighs) on the human body. Fig. 11(d-f) represents the bending scenario with approximate curvature radii (r) of the human body parts: 85 mm (wrist), 150 mm (biceps), and 250 mm (thigh). The simulated $|S_{11}|$ comparison is

plotted in Fig. 12(b). The proposed wearable antenna seems to be robust as both, the overall impedance bandwidth and input impedance throughout the bandwidth stays intact; even though an increase in bending angle decreases the effective resonating length which could shift the resonant frequency. Hence, the comparative results ensure that changing the location (on human body) of operation will not hamper the resonance characteristics of our wearable system.

IV. FABRICATION AND MEASUREMENT

This section presents the comparison of simulated and measured performance characteristics of the reported antenna (Ant-6) in the vicinity of modeled integrated circuit system. The circuit components are assembled at the backside of the antenna where battery (cell) is metallic and other components are PCB board models cased with dielectric (PVC) cover. Further, the whole integrated system is packaged with the biocompatible Polyimide layer and SMA connector (Female-Co-795-D) is used for power delivery. The fabricated prototype of the reported antenna with integrated system and the near-field (reflection coefficient) measurement setup (mimic the simulation scenario) in the laboratory environment is shown in Fig. 13.

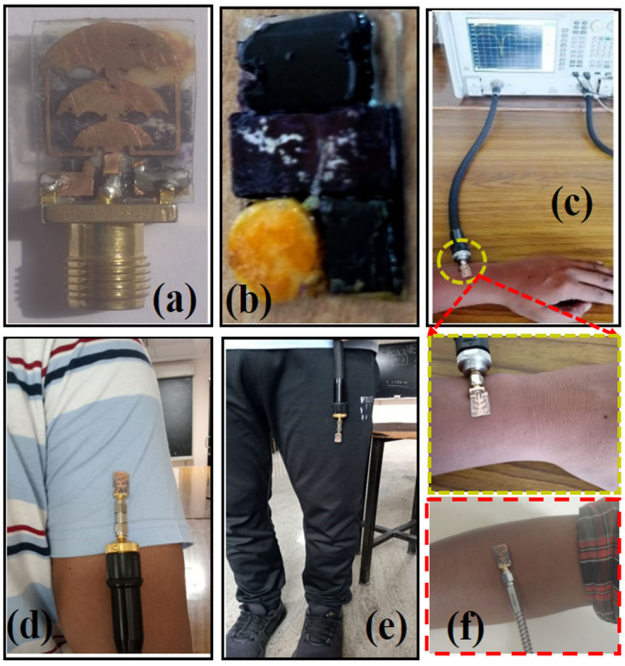

FIGURE 13. Experimental setup (a) Fabricated prototype with integrated circuit, (b) assembled electronic circuitry (c) near-field measurement setup for on-wrist scenario, (d) on-bicep scenario and, (e) on-thigh scenario, (f) on-forearm for validation of flexible characteristics.

For validation of the simulated results, Anritsu vector network analyzer (VNA) is used to perform the measurement of S-parameters in different scenarios, where the fabricated wearable patch prototype is placed on the wrist, biceps and thigh of the volunteer subject (human body). Fig. 14(a-b) presents the comparison of simulated and measured $|S_{11}|$ in different scenarios as discussed above. It is noticed that the measured impedance bandwidth for the proposed antenna (Ant-6) in free space scenario follows the simulation behavior in close proximity. It is also observed that for on-wrist, on-bicep, and on-thigh scenario, the proposed antenna seems to be robust as measured $|S_{11}|$ is not deflecting considerably from the simulation, and the overall $|S_{11}|$ behavior is also preserved throughout the bandwidth (UWB) even though the circuit assembling and packaging is done manually and prone to human handling and fabrication errors. Noted, in measurement the proposed wearable patch is placed at 0.25 mm height (thickness of fabric) above the skin surface in case of on-bicep, and on-thigh scenario; whereas for on-wrist scenario the wearable patch is placed just on the bare skin surface of the volunteer. The relative permittivity (typical range, 1.0-2.1) of the conventional fabric layer such as cotton, polyester, and nylon beneath the wearable patch is also believed to influence the $|S_{11}|$ of the antenna. In a comparable manner, the validation of the flexible characteristics for the proposed antenna for real-time applications is demonstrated by placing the antenna structure on the forearm, as illustrated in Fig. 13(f). The measured behavior of $|S_{11}|$ is compared in Fig. 14(a). Table 3 summarizes the simulated and measured -10 dB bandwidth for all the scenarios where, the comparable bandwidth results promisingly validate the strong robustness of the suggested wearable system.

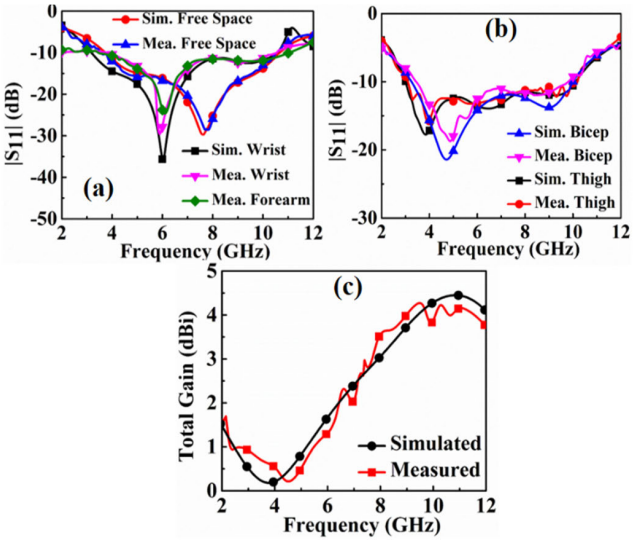

FIGURE 14. Comparison of simulated and measured performance (a, and b) $|S_{11}|$ for different scenarios, and (c) Total gain.

For far-field gain calculation, the measurement system in anechoic chamber is used, as shown in Fig. 15. In an anechoic chamber, the antenna under test (AUT) is positioned at distance $>$ 3m from the reference standard horn antenna (for UWB spectrum) to measure the radiation characteristics (plane, $\varphi = \theta = 0°$) of the antenna in the proposed wearable patch system. Noteworthy, to avoid the risk of EM radiations on the volunteer subject (human body), antenna system is placed over the customized four-layer phantom

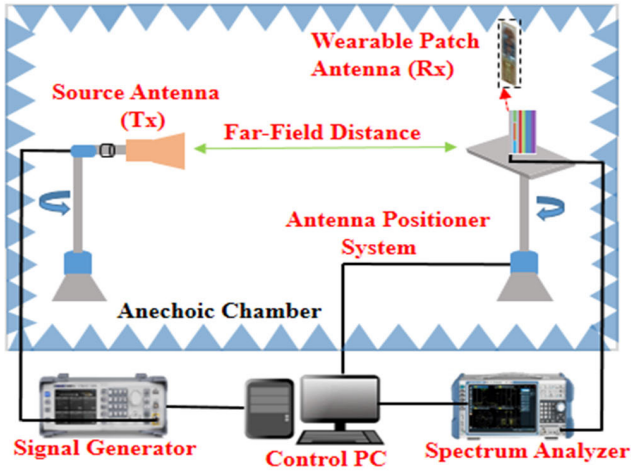

FIGURE 15. Schematic of far-field measurement set-up in an anechoic chamber, where AUT (proposed wearable patch) resides on the customized tissue mimicking four-layer phantom.

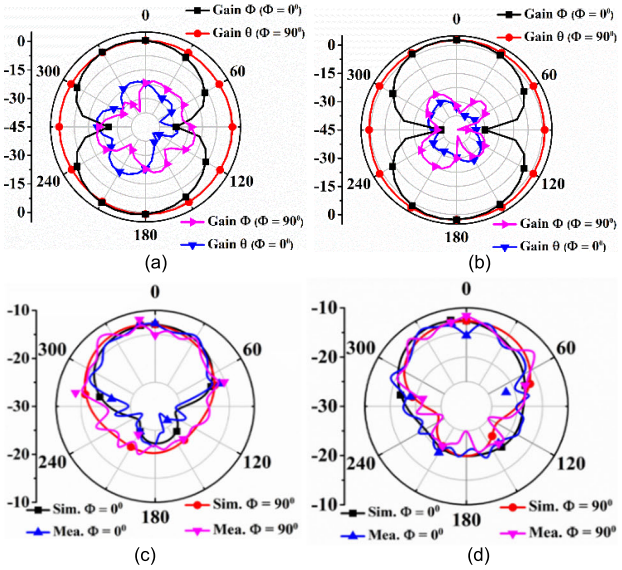

FIGURE 16. Far-field patterns at 5.8 GHz (left side) and 9.0 GHz (right side); (a-b) simulated co-pol. and cross-pol. patterns (gain) without circuitry, (c-d) comparison of simulated and measured co-pol. patterns (received power) with circuitry.

TABLE 3. Comparison of impedance bandwidth.

Sim. Enclosure	Free Space	Wrist	Bicep	Thigh
Sim. $\|S_{11}\|$ (GHz)	3.95-10.62	3.15-10.55	3.16-10.12	3.01-10.21
Meas. $\|S_{11}\|$ (GHz)	3.9-10.59	3.34-10.51	3.31-9.98	3.07-10.24

which emulates the skin-fat-muscle-bone tissue culture to mimic the rough approximation of on-wrist configuration (same as simulation enclosure). The phantom recipe formulation is referenced from the co-author's [37] but for this measurement setup the ingredients' proportion is scaled to obtain the average electrical properties in the UWB spectrum (3.1 – 10.6 GHz). The relative permittivity and conductivity of the tissue phantom is measured by dielectric probe (open ended high temperature probe) measurement kit (Keysight's 85070E). The total gain of the proposed wearable patch is shown in Fig. 14(c). The simulated and measured gain curves of the reported antenna are comparable and showing exponential increment throughout the frequency band. At 10.4 GHz, peak gain of 4.2 dBi, whereas, at 3.8 GHz lowest gain of 0.3 dBi is observed. This exponential behavior of the gain curve is believed to be activated due to the radiation from different surface areas on the antenna.

As evident from Fig. 8, currents with varying intensities are localized on different surface areas at different modes throughout the UWB spectrum. Fig. 16(a-b) outlines the simulated far-field radiation characteristics (gain) of the proposed on-body antenna system in the absence of integrated circuitry. Noted, gain $\boldsymbol{\Phi}(\boldsymbol{\Phi} = 0°)$ and gain $\boldsymbol{\theta}(\boldsymbol{\Phi} = 90°)$ are the co-polarized, whereas gain $\boldsymbol{\Phi}(\boldsymbol{\Phi} = 90°)$ and gain $\boldsymbol{\theta}(\boldsymbol{\Phi} = 0°)$ are the cross-polarized patterns. Without circuitry, radiation of the proposed antenna is bidirectional. Fig. 16(c-d) outlines the comparison of simulated and measured co-polarized far-field radiation characteristics (received power) of the proposed on-body antenna system in the presence of integrated circuitry, in both E-plane ($\boldsymbol{\Phi} = 0°$) and H-plane ($\boldsymbol{\Phi} = 90°$); at two different frequencies within the achieved UWB spectrum. Circuitry is acting as a reflector and thus, maximum radiation is in the broadside direction ($°\boldsymbol{\theta} = \mathbf{0}$).

V. SPECIFIC ABSORPTION RATE

The proposed on-body antenna is designed to operate just above the bare skin of the human body; thus, the EM radiations of the antenna could raise the temperature of the circumambient tissue cells and pose the life-threatening issues. The dosimetry quantity, specific absorption rate (SAR) quantifies the rate of EM radiations exposed to the body. In this work, the average SAR (ASAR) is evaluated numerically in the simulator when the prototype (antenna without integrated circuit) is placed just above (no gap) the bare skin of the anatomical HFSS model (wrist, biceps, thighs). Noted, the comparative analysis is also done with the 0.25 mm gap to account for the presence of fabric layer ($\boldsymbol{\varepsilon}_r = 1.0 - 2.1$) between the skin surface and the wearable prototype. In this regard, the ASAR calculation for the suggested antenna is performed at the central frequency of the targeted ultra-wideband (5.8 GHz) based on the anatomical model, consisting of tissue layers: skin, fat, muscles, and bone. As the typical wearable devices could be delivered maximum input power of 50 mW, therefore, for the on-wrist scenario (no gap case) the simulated 1-g and 10-g ASAR value is 1.99 W/Kg and 1.56 W/Kg respectively. The ASAR distribution on human wrist is shown in Fig. 17(a-b). For on-biceps and on-thighs case, SAR distribution is not shown for brevity but, the calculations are summarized in Table 4. The tabulated data shows that the thigh tissues are highly penetrated by the EM radiations, thereby, gives the highest ASAR values.

As per the IEEE, FCC, and ICNIRP guidelines [26], ASAR is restricted to 1.6 W/Kg and 2 W/Kg for 1 g and 10 g

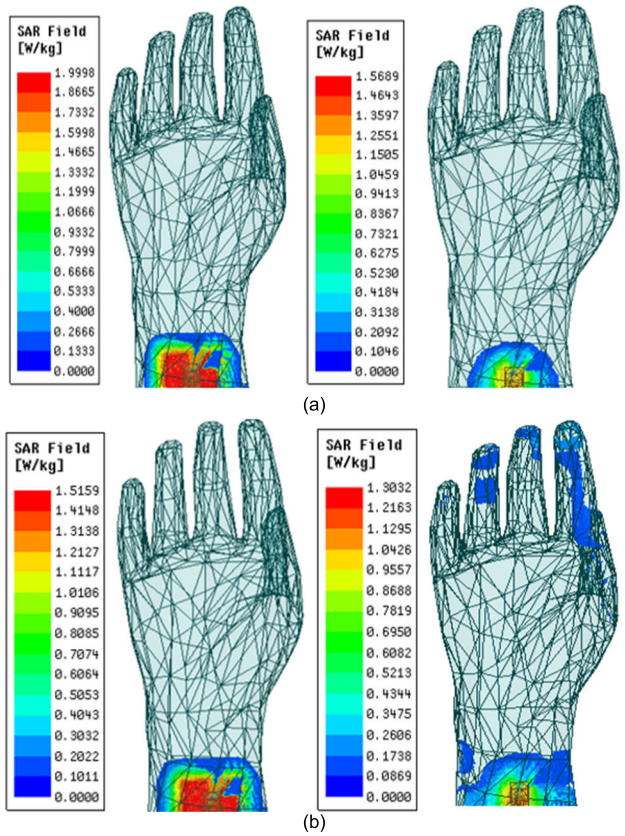

FIGURE 17. Simulated ASAR distribution at 5.8 GHz for the on-wrist scenario, (a) no gap, and (b) 0.25 mm gap case.

of cubic tissue, respectively. To meet such guidelines, max. input power that could be delivered to the proposed antenna are given in Table 4 for thigh tissues. As the transmitter power delivered to the wearable devices is in the order of 0.1 mW [38] which is even less than 1% of the maximum input power (see Table 4) needed for the proposed wearable antenna to reach the SAR limits. Therefore, the reported antenna can be a strong contender for practical use in wearable wireless systems operated within the UWB frequency bands.

TABLE 4. SAR values for different body parts.

Body Parts			Wrist	Biceps	Thigh	Input Power
SAR (W/Kg)	Gap (0 mm)	1-g	1.99	1.96	2.04	78.43
		10-g	1.56	1.51	1.62	123.45
	Gap (0.25 mm)	1-g	1.51	1.49	1.57	101.91
		10-g	1.30	1.27	1.44	138.88

Max. input power: mW (values given for only thigh tissues for briefness).

VI. CONCLUSION

Ultra-miniaturized umbrella-shaped UWB antenna bearing body-worn wearable patch has been designed and fabricated in this paper for health care monitoring applications. Based on the principle of characteristics mode theory, wideband behavior has been studied. The performance has been examined in terms of resonating frequency, operating bandwidth, average SAR, surface current distribution, radiation pattern, and gain. Further, parametric studies regarding robustness of the proposed wearable patch has also been carried out to monitor the sensitivity issues. It is concluded that the reported antenna is ultra-compact and has flexible geometry that can easily adapt to the curvature of the human body. Such wearable characteristics render the reported prototype an excellent candidate for e-healthcare monitoring applications in both indoor and outdoor environments.

ACKNOWLEDGMENT

(Sumon Modak and Vikrant Kaim are co-first authors.)

REFERENCES

[1] S. Modak and T. Khan, "A slotted UWB-MIMO antenna with quadruple band-notch characteristics using mushroom EBG structure," *AEU-Int. J. Electron. Commun.*, vol. 134, May 2021, Art. no. 153673.
[2] F. C. Commission, "Revision of—Part 15 of the commission's rules regarding ultra-wideband transmission systems," First Rep. Order, Washington, DC, USA, Tech. Rep., FCC 02–48, 2002.
[3] M. L. Meena, M. Kumar, G. Parmar, and R. S. Meena, "Design analysis and modeling of directional UWB antenna with elliptical slotted ground structure for applications in C- & X-bands," *Prog. Electromagn. Res. C*, vol. 63, pp. 193–207, 2016.
[4] R. Eshtiaghi, J. Nourinia, and C. Ghobadi, "Electromagnetically coupled band-notched elliptical monopole antenna for UWB applications," *IEEE Trans. Antennas Propag.*, vol. 58, no. 4, pp. 1397–1402, Apr. 2010.
[5] A. M. Abbosh and M. E. Bialkowski, "Design of ultrawideband planar monopole antennas of circular and elliptical shape," *IEEE Trans. Antennas Propag.*, vol. 56, no. 1, pp. 17–23, Jan. 2008.
[6] M. Rahanandeh, A. S. Noor Amin, M. Hosseinzadeh, P. Rezai, and M. S. Rostami, "A compact elliptical slot antenna for covering Bluetooth/WiMAX/WLAN/ITU," *IEEE Antennas Wireless Propag. Lett.*, vol. 11, pp. 857–860, 2012.
[7] E. S. Angelopoulos, A. Z. Anastopoulos, D. I. Kaklamani, A. A. Alexandridis, F. Lazarakis, and K. Dangakis, "Circular and elliptical CPW-fed slot and microstrip-fed antennas for ultrawideband applications," *IEEE Antennas Wireless Propag. Lett.*, vol. 5, pp. 294–297, 2006.
[8] Y. Yan, Y. Jiao, Z. Weng, and C. Zhang, "An umbrella-shaped broadband circularly polarized antenna with wide beamwidth for global navigation satellite systems applications," *Microw. Opt. Technol. Lett.*, vol. 61, no. 11, pp. 2455–2462, Nov. 2019.
[9] S. Kundu, A. Chatterjee, S. K. Jana, and S. K. Parui, "A compact umbrella-shaped UWB antenna with gain augmentation using frequency selective surface," *Radioengineering*, vol. 27, no. 2, pp. 448–454, Jun. 2018.
[10] D. N. Elsheakh, H. A. Elsadek, E. A. Abdallah, M. F. Iskander, and H. Elhenawy, "Ultrawide bandwidth umbrella-shaped microstrip monopole antenna using spiral artificial magnetic conductor (SAMC)," *IEEE Antennas Wireless Propag. Lett.*, vol. 8, pp. 1255–1258, 2009.
[11] M. Kanagasabai, P. Sambandam, M. G. N. Alsath, S. Palaniswamy, A. Ravichandran, and C. Girinathan, "Miniaturized circularly polarized UWB antenna for body centric communication," *IEEE Trans. Antennas Propag.*, vol. 70, no. 1, pp. 189–196, Jan. 2022.
[12] A. Y. I. Ashyap, Z. Z. Abidin, S. H. Dahlan, H. A. Majid, and F. C. Seman, "A compact wearable antenna using ebg for smart-watch applications," in *Proc. Asia–Pacific Microw. Conf. (APMC)*, 2018, pp. 1477–1479. [Online]. Available: www.cst.com
[13] D. Wu and S. W. Cheung, "A cavity-backed annular slot antenna with high efficiency for smartwatches with metallic housing," *IEEE Trans. Antennas Propag.*, vol. 65, no. 7, pp. 3756–3761, Jul. 2017.
[14] R. Rabhi, S. Gahgouh, and A. Gharsallah, "Watchstrap integrated wideband circularly polarized antenna design for smartwatch applications," *IET Microw., Antennas Propag.*, vol. 16, no. 9, pp. 587–601, Jul. 2022.
[15] B. Fady, A. Tribak, J. Terhzaz, and F. Riouch, "Novel low-cost integrated multiband antenna design customized for smartwatch applications with SAR evaluation," *Int. J. Antennas Propag.*, vol. 2020, pp. 1–14, Dec. 2020.

[16] Y. Chen and T. Ku, "A low-profile wearable antenna using a miniature high impedance surface for smartwatch applications," *IEEE Antennas Wireless Propag. Lett.*, vol. 15, pp. 1144–1147, 2016.
[17] D. Wen, Y. Hao, H. Wang, and H. Zhou, "Design of a MIMO antenna with high isolation for smartwatch applications using the theory of characteristic modes," *IEEE Trans. Antennas Propag.*, vol. 67, no. 3, pp. 1437–1447, Mar. 2019.
[18] C.-H. Wu, J.-S. Sun, and B.-S. Lu, "Watchstrap-embedded four-element multiple-input-multiple-output antenna design for a smartwatch in 5.2–5.8 GHz wireless applications," *Int. J. Antennas Propag.*, vol. 2018, pp. 1–16, Jan. 2018.
[19] K. N. Paracha, S. K. A. Rahim, P. J. Soh, and M. Khalily, "Wearable antennas: A review of materials, structures, and innovative features for autonomous communication and sensing," *IEEE Access*, vol. 7, pp. 56694–56712, 2019.
[20] S. Sankaralingam and B. Gupta, "Determination of dielectric constant of fabric materials and their use as substrates for design and development of antennas for wearable applications," *IEEE Trans. Instrum. Meas.*, vol. 59, no. 12, pp. 3122–3130, Dec. 2010.
[21] A. Rahman, M. T. Islam, M. J. Singh, S. Kibria, and M. Akhtaruzzaman, "Electromagnetic performances analysis of an ultra-wideband and flexible material antenna in microwave breast imaging: To implement a wearable medical bra," *Sci. Rep.*, vol. 6, no. 1, p. 38906, Dec. 2016.
[22] S. Parameswari and C. Chitra, "Textile UWB antenna with metamaterial for healthcare monitoring," *Int. J. Antennas Propag.*, vol. 2021, pp. 1–11, Dec. 2021.
[23] S. Jayant, G. Srivastava, and S. Kumar, "Quad-port UWB MIMO footwear antenna for wearable applications," *IEEE Trans. Antennas Propag.*, vol. 70, no. 9, pp. 7905–7913, Sep. 2022.
[24] M. El Atrash, M. A. Abdalla, and H. M. Elhennawy, "A wearable dual-band low profile high gain low SAR antenna AMC-backed for WBAN applications," *IEEE Trans. Antennas Propag.*, vol. 67, no. 10, pp. 6378–6388, Oct. 2019.
[25] I. A. Shah, M. Zada, and H. Yoo, "Design and analysis of a compact-sized multiband spiral-shaped implantable antenna for scalp implantable and leadless pacemaker systems," *IEEE Trans. Antennas Propag.*, vol. 67, no. 6, pp. 4230–4234, Jun. 2019, doi: 10.1109/TAP.2019.2908252.
[26] S. Kumar, D. Nandan, K. Srivastava, S. Kumar, H. Singh, M. Marey, H. Mostafa, and B. K. Kanaujia, "Wideband circularly polarized textile MIMO antenna for wearable applications," *IEEE Access*, vol. 9, pp. 108601–108613, 2021.
[27] M. Yousaf, I. B. Mabrouk, M. Zada, A. Akram, Y. Amin, M. Nedil, and H. Yoo, "An ultra-miniaturized antenna with ultra-wide bandwidth characteristics for medical implant systems," *IEEE Access*, vol. 9, pp. 40086–40097, 2021.
[28] P. P. Shome, T. Khan, A. A. Kishk, and Y. M. M. Antar, "Quad-element MIMO antenna system using half-cut miniaturized UWB antenna for IoT-based smart home digital entertainment network," *IEEE Internet Things J.*, vol. 10, no. 20, pp. 17964–17976, Oct. 2023.
[29] A. Iqbal, A. Bouazizi, S. Kundu, I. Elfergani, and J. Rodriguez, "Dielectric resonator antenna with top loaded parasitic strip elements for dual-band operation," *Microw. Opt. Technol. Lett.*, vol. 61, no. 9, pp. 2134–2140, Sep. 2019.
[30] A. Altaf, A. Iqbal, A. Smida, J. Smida, A. A. Althuwayb, S. Hassan Kiani, M. Alibakhshikenari, F. Falcone, and E. Limiti, "Isolation improvement in UWB-MIMO antenna system using slotted stub," *Electronics*, vol. 9, no. 10, p. 1582, Sep. 2020.
[31] Y. Chen and C. F. Wang, *Characteristic Modes: Theory and Applications in Antenna Engineering*. Hoboken, NJ, USA: Wiley, 2015, pp. 1–263.
[32] M. Vogel, G. Gampala, D. Ludick, U. Jakobus, and C. J. Reddy, "Characteristic mode analysis: Putting physics back into simulation," *IEEE Antennas Propag. Mag.*, vol. 57, no. 2, pp. 307–317, Apr. 2015.
[33] A. Sharma, D. Gangwar, R. P. Singh, R. Solanki, S. Rajpoot, B. K. Kanaujia, S. P. Singh, and A. Lay-Ekuakille, "Design of compact wideband circularly polarized hexagon-shaped antenna using characteristics mode analysis," *IEEE Trans. Instrum. Meas.*, vol. 70, pp. 1–8, 2021.
[34] C. Wang, Y. Chen, and S. Yang, "Bandwidth enhancement of a dual-polarized slot antenna using characteristic modes," *IEEE Antennas Wireless Propag. Lett.*, vol. 17, no. 6, pp. 988–992, Jun. 2018.
[35] C. Fu, C. Feng, W. Chu, Y. Yue, X. Zhu, and W. Gu, "Design of a broadband high-gain omnidirectional antenna with low cross polarization based on characteristic mode theory," *IEEE Antennas Wireless Propag. Lett.*, vol. 21, pp. 1747–1751, 2022.
[36] R. J. Garbacz and R. Turpin, "A generalized expansion for radiated and scattered fields," *IEEE Trans. Antennas Propag.*, vol. AP-19, no. 3, pp. 348–358, May 1971.
[37] V. Kaim, B. K. Kanaujia, and K. Rambabu, "Quadrilateral spatial diversity circularly polarized MIMO cubic implantable antenna system for biotelemetry," *IEEE Trans. Antennas Propag.*, vol. 69, no. 3, pp. 1260–1272, Mar. 2021.
[38] A. Iqbal, A. Smida, A. J. Alazemi, M. I. Waly, N. K. Mallat, and S. Kim, "Wideband circularly polarized MIMO antenna for high data wearable biotelemetric devices," *IEEE Access*, vol. 8, pp. 17935–17944, 2020.

SUMON MODAK (Member, IEEE) received the B.Tech. degree in electronics and communication engineering from Dr. M. G. R. University (A Deemed University), Chennai, Tamil Nadu, India, the M.Tech. degree in communication system engineering from Sambalpur University (SUIIT), Sambalpur, Odisha, India, and the Ph.D. degree in electronics and communication engineering from the National Institute of Technology Silchar, Assam, India. He is currently a Postdoctoral Fellow with the Department of Electronics and Communication Engineering, National Institute of Technology Warangal, Telangana, India. His current research interests include UWB and millimeter-wave antennas, EBG structures, CMA, and implantable antenna for biomedical applications.

VIKRANT KAIM (Member, IEEE) received the Ph.D. degree in electronics and communication from Jawaharlal Nehru University, New Delhi, India, in 2022. From January 2023 to December 2023, he was a Postdoctoral Fellow with the Department of Electrical and Computer Engineering, University of Alberta, Edmonton, Canada. In December 2023, he joined the Department of Electronics and Communication Engineering, Faculty of Technology, University of Delhi, New Delhi, India, as an Assistant Professor. His research interests include electromagnetic theory, implantable antennas and devices, wireless power transfer, retinal prosthesis, cardiac implants, and capsule endoscopy. He was a recipient of the prestigious CSIR Senior Research Fellowship, in 2019. He is serving as a Reviewer for IEEE TRANSACTIONS ON ANTENNAS AND PROPAGATION, IEEE TRANSACTIONS ON MICROWAVE THEORY AND TECHNIQUES, and IEEE TRANSACTIONS ON BIOMEDICAL ENGINEERING.

TAIMOOR KHAN (Senior Member, IEEE) received the Diploma (Polytechnic) degree in electronics engineering from the Board of Technical Education, Uttar Pradesh, India, in 2001, the Graduate degree in electronics and communication engineering from the Institution of Engineers, Kolkata, India, in 2005, the master's degree in communication engineering from the Shobhit Institute of Engineering and Technology, Meerut, India, in 2009, and the Ph.D. degree in electronics and communication engineering from the National Institute of Technology Patna, India, in 2014. He is currently an Associate Professor with the Department of Electronics and Communication Engineering, National Institute of Technology Silchar, India. His research interests include printed microwave and millimeter-wave circuits, electromagnetic bandgap structures, dielectric resonator antennas, and artificial intelligence paradigms in electromagnetics.

BINOD KUMAR KANAUJIA (Senior Member, IEEE) received the B.Tech. degree in electronics engineering from the Kamla Nehru Institute of Technology (KNIT), Sultanpur, India, in 1994, and the M.Tech. and Ph.D. degrees from the Department of Electronics Engineering, IIT (Banaras Hindu University) Varanasi, Varanasi, India, in 1998 and 2004, respectively. He has been a Professor and the Dean of the School of Computational and Integrative Sciences, Jawaharlal Nehru University (JNU), New Delhi, India, since August 2016, and the Director (Deputation) of the Dr. B. R. Ambedkar National Institute of Technology Jalandhar (NIT Jalandhar), Jalandhar, India, since February 2022. He has also been with the Department of Electronics and Communication Engineering, Ambedkar Institute of Advanced Communication Technologies and Research (formerly, Ambedkar Institute of Technology), as a Professor, since February 2011, where he was an Associate Professor, from 2008 to 2011. He held the positions of the Dean, SC and IS, and the Chief Advisor of the Equal Opportunity Office, JNU. Prior to this, he held the positions of Lecturer, from 1996 to 2005, a Reader, from 2005 to 2008, and the Head of the Department of Electronics and Communication Engineering, M. J. P. Rohilkhand University, Bareilly, India. Prior to his career in academics, he was an Executive Engineer with the Research and Development Division, M/s Uptron India Ltd. He has been credited with publishing more than 400 research papers, three books, 11 book chapters, and ten patents with more than 4600 citations with an H-index of 32 in several peer-reviewed journals and conferences. He had supervised 50 M.Tech. and 35 Ph.D. research scholars in the field of microwave engineering. His research interests include the design and modeling of microstrip antenna, dielectric resonator antenna, left-handed metamaterial microstrip antenna, shorted microstrip antenna, ultra-wideband antennas, and reconfigurable, and circular polarized antennas for wireless communication. He is a member of several academic and professional bodies, such as the Indian Society for Technical Education, and a fellow of the Institution of Engineers, India, and the Institute of Electronics and Telecommunication Engineers of India. He has successfully executed six research projects with three ongoing projects sponsored by several agencies of the Government of India, such as DRDO, DST, DBT, SERB, AICTE, and ISRO. He has been awarded the Junior Research Fellowship by UGC Delhi for his outstanding work in the electronics field, from 2001 to 2002. He is a Reviewer for several journals of international repute, such as *IET Microwaves, Antennas and Propagation*, IEEE Antennas and Wireless Propagation Letters, *Wireless Personal Communications*, *Journal of Electromagnetic Wave and Application*, *Indian Journal of Radio and Space Physics*, *IETE Technical Review*, *International Journal of Electronics*, *International Journal of Engineering Science*, IEEE Transactions on Antennas and Propagation, *AEU-International Journal of Electronics and Communication*, and *International Journal of Microwave and Wireless Technologies*. He is also an Associate Editor of IEEE Access and an Editor of *AEU-International Journal of Electronics and Communication* (Elsevier) and *IETE Technical Review* (Taylor and Francis).

LADISLAU MATEKOVITS (Senior Member, IEEE) received the degree in electronic engineering from the Institutul Politehnic din Bucureşti, Bucureşti, Romania, in 1992, and the Ph.D. degree (Dottorato di Ricerca) in electronic engineering from Politecnico di Torino, Turin, Italy, in 1995. Since 1995, he has been with the Department of Electronics and Telecommunications, Politecnico di Torino, first with a Postdoctoral Fellowship and then as a Research Assistant. In 2002, he joined the Department of Electronics and Telecommunications, Politecnico di Torino, as an Assistant Professor. In 2005, he was appointed as a Senior Assistant Professor and an Associate Professor, in 2014. In 2005, he was a Visiting Scientist with the Department of Antennas and Scattering, FGAN-FHR (now Fraunhofer Institute), Wachtberg, Germany. In July 2009, he joined Macquarie University, Sydney, NSW, Australia, as a Marie Curie Fellow, for two years, where he also held a visiting academic position, in 2013. In 2014, he was an Associate Professor and appointed as an Honorary Fellow. In February 2017, he was a Full Professor in Italy. Since 2020, he has been an Honorary Professor with the Polytechnic University of Timisoara, Romania, and an Associate Professor with the Italian National Research Council. He has been invited to serve as a research grant assessor for government funding calls (Romania, Italy, Croatia, and Kazakhstan) and as an international expert in Ph.D. thesis evaluation by several universities from Australia, India, Pakistan, and Spain. He has published more than 400 articles, including more than 125 journal contributions, and delivered seminars on these topics all around the world: Europe, USA (AFRL/MIT-Boston), Australia, China, and Russia. His main research interests include numerical analysis of printed antennas and in particular development of new, numerically efficient full-wave techniques to analyze large arrays, and active and passive metamaterials for cloaking applications. Material parameter retrieval of these structures by inverse methods and different optimization techniques has also been considered. In the last years, bio-electromagnetic aspects have also been contemplated, such as example design of implantable antennas or the development of nano-antennas for example for drug delivery applications. He has been a member of the Organizing Committee of the International Conference on Electromagnetics in Advanced Applications (ICEAA), since 2010. He was appointed as a member of the National Council for the Attestation of University Degrees, Diplomas and Certificates (CNATDCU), Romania, from 2020 to 2024. He is a member of the technical program committee member of several conferences. He was a recipient of various awards in international conferences, including the 1998 URSI Young Scientist Award, Thessaloniki, Greece; the Barzilai Award 1998 (Young Scientist Award, granted every two years by the Italian National Electromagnetic Group); and the Best AP2000 Oral Paper on Antennas, ESA-EUREL Millennium Conference on Antennas and Propagation, Davos, Switzerland. He was a recipient of the Motohisa Kanda Award, in 2018, for the most cited paper of IEEE Transactions on Electromagnetic Compatibility in the past five years. He received the 2019 American Romanian Academy of Arts and Sciences (ARA) Medal of Excellence in Science; the Ad Astra Award, in 2020; and a Senior Researcher for Excellence in Research. He has been the Assistant Chairperson and the Publication Chairperson of the European Microwave Week 2002, Milan, Italy; and the General Chair of the 11th International Conference on Body Area Networks (BodyNets 2016). He serves as an Associate Editor for IEEE Transactions on Antennas and Propagation, IEEE Access, IEEE Antennas and Wireless Propagation Letters, and *IET MAP*, and a reviewer for different journals.

KARUMUDI RAMBABU (Member, IEEE) received the Ph.D. degree in electrical and computer engineering from the University of Victoria, Victoria, BC, Canada, in 2005. From 2005 to 2007, he was a Research Member with the Institute for Infocomm Research, Singapore. Since 2007, he has been an Assistant Professor with the Department of Electrical and Computer Engineering, University of Alberta, Edmonton, AB, Canada, where he is currently a Professor. He is also involved in oil well monitoring, pipeline inspection, through-wall imaging, vital sign monitoring, and biopsy needle guiding using ultrawideband (UWB) radar systems. His current research interests include the design and development of UWB technology, and components and systems for various applications. He was a recipient of the Andy Farquharson Award for excellence in graduate student teaching from the University of Victoria, in 2003, and the Governor General's Gold Medal for the Ph.D. research, in 2005. He serves as an Associate Editor for the *IET Microwaves, Antennas and Propagation*.

Open Access funding provided by 'Politecnico di Torino' within the CRUI CARE Agreement